Collective modes of doped graphene and a standard two-dimensional electron gas in a strong magnetic field: Linear magnetoplasmons versus magnetoexcitons

R. Roldán, J.-N. Fuchs, and M. O. Goerbig
Laboratoire de Physique des Solides, Université Paris-Sud, CNRS, UMR 8502, F-91405 Orsay Cedex, France
(Received 18 March 2009; revised manuscript received 17 June 2009; published 6 August 2009)

A doped graphene layer in the integer quantum-Hall regime reveals a highly unusual particle-hole excitation spectrum, which is calculated from the dynamical polarizability in the random-phase approximation. We find that the elementary neutral excitations in graphene in a magnetic field are unlike those of a standard two-dimensional electron gas: in addition to the upper-hybrid mode, the particle-hole spectrum is reorganized in linear magnetoplasmons that disperse roughly parallel to $\omega = v_F q$, instead of the usual horizontal (almost dispersionless) magnetoexcitons. These modes could be detected in an inelastic light-scattering experiment.

DOI: 10.1103/PhysRevB.80.085408 PACS number(s): 73.43.Lp, 78.30.Na, 81.05.Uw

I. INTRODUCTION

Particle-hole excitations in a standard two-dimensional electron gas are incoherent and form a continuum in the energy-momentum plane.[1,2] This continuum does not have a uniform weight but features some structure that hints at possible coherent excitations. If one includes interactions between the electrons, coherent excitations may emerge from the continuum. This is the case of the plasmon, which appears once long-range Coulomb interactions are taken into account. The plasmon mode is long lived outside the continuum but it is Landau damped once it penetrates it. If instead of including interactions, one turns on a magnetic field, the electronic energy is quenched into Landau levels (LLs), and the particle-hole continuum becomes discrete in energy, while remaining essentially continuous in the momentum direction. When both the magnetic field and Coulomb interactions are considered, the continuum is reorganized in magnetoexcitons—transverse excitations that now acquire a dispersion[3]—and an upper-hybrid mode[4] exists outside what used to be the continuum.

Graphene, a recently discovered carbon material, is attracting a lot of interest due to its unique electronic properties (see Ref. 5). Electrons in graphene may be viewed as a particular form of the two-dimensional electron gas (2DEG). However, due to its underlying triangular lattice with a two-atom basis, the electrons of graphene are described by a massless Dirac equation instead of the usual effective-mass Schrödinger equation. The screening properties of graphene are different from that of the 2DEG, as it may be seen from the polarization and dielectric functions in the two cases.[6–10] Furthermore, the single-particle spectral function reveals the particular chiral properties of the Dirac-type quasiparticles.[11,12] Another salient physical consequence is a peculiar integer quantum-Hall effect.[13,14]

In this paper, we show that collective excitations of graphene in a strong magnetic field are much unlike that of the standard 2DEG (from now on, we use the term 2DEG to denote a standard 2DEG with a parabolic band dispersion, in contrast to graphene). The magnetic field also reorganizes the particle-hole continuum but instead of revealing horizontal lines, diagonal lines emerge. When Coulomb interactions are included within the random-phase approximation (RPA), the diagonal excitations acquire coherence. We shall refer to them as *linear magnetoplasmons* in order to distinguish them from the *upper-hybrid mode*—which is also present and which may be considered as the plasmon mode modified by the magnetic field—and from the usual (horizontal) *magnetoexcitons*, which are blurred in graphene. Several recent theoretical works considered collective excitations in graphene in a magnetic field, concentrating either on magnetoexcitons[15–17] or on the plasmon mode.[18,19] Here, we show that concentrating on horizontal magnetoexcitons, in spite of its success in the 2DEG,[3] is not sufficient to reveal the complete structure of the particle-hole excitation spectrum (PHES) in graphene, which is dominated by linear magnetoplasmons that disperse roughly parallel to $\omega = v_F q$.

The paper is organized as follows. In Sec. II we calculate the polarization function of a 2DEG and that of doped graphene in the integer quantum-Hall regime. In Sec. III we discuss the main features of the noninteracting PHES of graphene and a 2DEG and the different nature of the collective modes in each case, once electron-electron interactions are taken into account. The conclusions are summarized in Sec. IV.

II. POLARIZATION FUNCTION

The polarization operator $\Pi(\mathbf{q},\omega)$ may be viewed as the particle-hole pair propagator, the poles of which yield the dispersion relation and damping of the collective excitations. Its imaginary part is related to the dynamical structure factor by

$$S(\mathbf{q},\omega) = -\frac{1}{\pi}\mathrm{Im}\,\Pi(\mathbf{q},\omega),$$

which plays the role of a spectral function for the particle-hole propagator. The PHES is defined as the (ω,q) region of nonzero spectral weight $S(\mathbf{q},\omega) \neq 0$. Peaks in the spectral density are interpreted as collective excitations; their dispersion relation and damping may be extracted from the position and the width of the peaks (see, e.g., Sec. 3.2.7. in Ref. 1).

The Fourier-transformed polarizability for noninteracting electrons (we use a unit system with $\hbar \equiv 1$)

$$\Pi^0(\mathbf{q},\omega) = \int \frac{d\omega' d\mathbf{k}}{i(2\pi)^3} \mathrm{Tr}[G^0(\mathbf{k},\omega')G^0(\mathbf{k}+\mathbf{q},\omega'+\omega)] \quad (1)$$

is given in terms of the free single-particle Green's functions $G^0(\mathbf{q},\omega)$. Whereas, as we review below, the single-particle Green's functions for the conventional 2DEG are simple scalar functions, those of graphene are 2×2 matrices due to the two sublattices A and B. The trace in Eq. (1) is, thus, relevant only in the case of graphene.

A. Polarizability in the 2DEG

The Hamiltonian for electrons in the conventional 2DEG is simply that of free electrons with a band mass m_b, $\mathcal{H} = \boldsymbol{\pi}^2/2m_b$, where the gauge-invariant momentum operators, $\boldsymbol{\pi} = \mathbf{p} + e\mathbf{A}(\mathbf{r})$ takes into account the coupling to the magnetic field $\mathbf{B} = \nabla \times \mathbf{A}$, where $\mathbf{A}$ is the vector potential. The operators $\boldsymbol{\pi}$ may be expressed in terms of the usual ladder operators with the help of

$$a = \frac{l_B}{\sqrt{2}}(\pi_x - i\pi_y), \quad a^\dagger = \frac{l_B}{\sqrt{2}}(\pi_x + i\pi_y),$$

which satisfy the commutation relations $[a,a^\dagger]=1$, and $l_B = 1/\sqrt{eB}$ is the magnetic length. One obtains the usual eigenstates, $|n,m\rangle$, and the eigenvalue equation $\mathcal{H}|n,m\rangle = \omega_c(n+1/2)|n,m\rangle$, where $\omega_c = 1/m_b l_B^2 = eB/m_b$ is the cyclotron frequency. The result is the usual LL spectrum where the levels are labeled by the quantum number n, the eigenvalue of $a^\dagger a$. The additional quantum number m is associated with the guiding center operator, and varies between 0 and $N_B - 1$, where $N_B = \mathcal{A}/2\pi l_B^2$, in terms of the sample area $\mathcal{A}$.

With the help of the eigenstates $|n,m\rangle$, one may express the Green's functions $G^0(\mathbf{q},\omega)$ for noninteracting electrons in Fourier space, as

$$G^0(\mathbf{q},\omega) = \sum_{n,m} \frac{\langle \mathbf{q}|n,m\rangle\langle n,m|\mathbf{r}=0\rangle}{\omega - \xi_n + i\delta\,\mathrm{sgn}(\xi_n)}, \quad (2)$$

where $\xi_n \equiv \omega_c(n+1/2) - \epsilon_F$ is the energy of the nth LL with respect to the Fermi energy ϵ_F, which we choose to lie between two LLs of the conduction band (integer quantum-Hall regime), and δ accounts for disorder-induced level broadening ($\delta \to 0^+$ in the clean limit).

Equation (2) allows us to calculate the polarization function (1) for the 2DEG

$$\Pi^0(\mathbf{q},\omega) = \sum_{n=0}^{N_F} \sum_{n'=N_F+1}^{\infty} \frac{F_{nn'}(\mathbf{q})}{(n-n')\omega_c + \omega + i\delta} + (\omega^+ \to \omega^-),$$

where N_F is the index of the last occupied LL, which is fixed by the filling factor, and $\omega^+ \to \omega^-$ indicates the replacement $\omega + i\delta \to -\omega - i\delta$. The form factors for the 2DEG read[1]

$$F_{nn'}(\mathbf{q}) = e^{-l_B^2 q^2/2}\left(\frac{l_B^2 q^2}{2}\right)^{n_>-n_<} \frac{n_<!}{n_>!}\left[L_{n_<}^{n_>-n_<}\left(\frac{l_B^2 q^2}{2}\right)\right]^2 \quad (3)$$

with $n_> \equiv \max\{n,n'\}$ and $n_< \equiv \min\{n,n'\}$, and L_n^m are associated Laguerre polynomials.

B. Polarizability in graphene

For graphene in a magnetic field, the electronic Hamiltonian may be written as[5]

$$\mathcal{H} = \frac{\sqrt{2}v_F}{l_B}\begin{pmatrix} 0 & a \\ a^\dagger & 0 \end{pmatrix}, \quad (4)$$

where $v_F = 3ta_{cc}/2$ is the Fermi velocity, in terms of the nearest-neighbor hopping integral $t \simeq 3$ eV, and the carbon-carbon distance $a_{cc} \simeq 1.4$ Å. Strictly speaking, Eq. (4) is only valid on one of the valleys, namely, K, that of the valley K' being $-\mathcal{H}^*$. However, we concentrate, here, only on processes that do not couple the two different valleys, such that a discussion of the Hamiltonian (4) is sufficient, and the twofold valley degeneracy may be accounted for by a simple factor of 2.

The Hamiltonian (4) yields the relativistic LL spectrum

$$\lambda\epsilon_n = \lambda\frac{v_F}{l_B}\sqrt{2n},$$

where λ denotes the band index, $\lambda = +$ for the conduction, and $\lambda = -$ for the valence band. The associated eigenstates are the 2 spinors

$$\psi_{\lambda,n,m} = \frac{1}{\sqrt{2}}\begin{pmatrix} |n-1,m\rangle \\ \lambda|n,m\rangle \end{pmatrix} \quad \text{for } n \geq 1,$$

$$\psi_{n=0,m} = \begin{pmatrix} 0 \\ |n=0,m\rangle \end{pmatrix} \quad \text{for } n = 0,$$

where $m = 0,1,\ldots,N_B-1$, and $|n,m\rangle$ are the corresponding eigenstates of the Hamiltonian with quadratic dispersion, introduced in the previous subsection. Due to the 2-spinor structure of the wave functions in graphene, the associated single-particle Green's functions are 2×2 matrices

$$G^0_{\zeta;\alpha\alpha'}(\mathbf{k},\omega) = \sum_\lambda \sum_n \frac{f_{\zeta,\alpha\alpha';\lambda n}(\mathbf{k}+\zeta\mathbf{K})}{\omega - \lambda\xi_n + i\delta\,\mathrm{sgn}(\lambda\xi_n)} \quad (5)$$

with $\alpha = A(B)$ for electrons on the $A(B)$ sublattice, $\zeta = +(-)$ for electrons in the $K(K')$ valley, and $\mathbf{k}$ is the electron momentum measured from the Dirac points, $\zeta\mathbf{K} = \zeta 4\pi/3\sqrt{3}a\mathbf{u}_x$. In the denominator, we have defined $\lambda\xi_n \equiv \lambda\epsilon_n - \epsilon_F$, the energy difference between the level $\lambda\epsilon_n$, and the Fermi energy ϵ_F. Furthermore, we neglect Zeeman and possible valley splittings. The matrix $f_{\lambda n}(\mathbf{q})$ for the K valley is

$$f_{K;\lambda n}(\mathbf{q}) = \sum_m \begin{pmatrix} 1_n^{*2}\langle \mathbf{q}|n-1,m\rangle\langle n-1,m|\mathbf{r}=0\rangle & -i\lambda 1_n^* 2_n^* \langle \mathbf{q}|n-1,m\rangle\langle n,m|\mathbf{r}=0\rangle \\ i\lambda 1_n^* 2_n^* \langle \mathbf{q}|n,m\rangle\langle n-1,m|\mathbf{r}=0\rangle & 2_n^{*2}\langle \mathbf{q}|n,m\rangle\langle n,m|\mathbf{r}=0\rangle \end{pmatrix}, \tag{6}$$

where we have introduced the simplified notation $1_n^* = \sqrt{(1-\delta_{n,0})/2}$, $2_n^* = \sqrt{(1+\delta_{n,0})/2}$. The bare polarization bubble is

$$\Pi^0(\mathbf{q},\omega) = \sum_{n=1}^{N_F} \Pi_n^{\lambda_F}(\mathbf{q},\omega) + \Pi^{vac}(\mathbf{q},\omega), \tag{7}$$

where the index N_F of the last occupied LL is now related to the filling factor ν by $\nu = 4N_F + 2$ due to the fourfold spin and valley degeneracy. There is a nonzero vacuum polarization, $\Pi^{vac}(\mathbf{q},\omega) \equiv -\Sigma_{n=1}^{N_c} \Pi_n^{\lambda=1}(\mathbf{q},\omega)$, the vacuum corresponding to undoped graphene. Here, N_c is an ultraviolet cutoff[20] and

$$\Pi_n^{\lambda}(\mathbf{q},\omega) = \sum_{\lambda'} \sum_{n'=0}^{n-1} \Pi_{nn'}^{\lambda\lambda'}(\mathbf{q},\omega) + \sum_{\lambda'} \sum_{n'=n+1}^{N_c} \Pi_{nn'}^{\lambda\lambda'}(\mathbf{q},\omega) + \Pi_{nn}^{\lambda-\lambda}(\mathbf{q},\omega). \tag{8}$$

In the previous expressions, we have used

$$\Pi_{nn'}^{\lambda\lambda'}(\mathbf{q},\omega) \equiv \frac{\overline{\mathcal{F}}_{nn'}^{\lambda\lambda'}(\mathbf{q})}{\lambda\xi_n - \lambda'\xi_{n'} + \omega + i\delta} + (\omega^+ \to \omega^-), \tag{9}$$

where the form factor is

$$\overline{\mathcal{F}}_{nn'}^{\lambda\lambda'}(\mathbf{q}) = e^{-l_B^2 q^2/2} \left(\frac{l_B^2 q^2}{2}\right)^{n_>-n_<} \times \left\{ \lambda 1_n^* 1_{n'}^* \sqrt{\frac{(n_<-1)!}{(n_>-1)!}} L_{n_<-1}^{n_>-n_<}\left(\frac{l_B^2 q^2}{2}\right) + \lambda' 2_n^* 2_{n'}^* \sqrt{\frac{n_<!}{n_>!}} L_{n_<}^{n_>-n_<}\left(\frac{l_B^2 q^2}{2}\right) \right\}^2. \tag{10}$$

Notice that Eq. (10) agrees with the form factor obtained in Ref. 17 but not with those obtained in Refs. 18 and 19. Because of the presence of nodes in the LL wave functions (zeros of the Laguerre polynomials), $\overline{\mathcal{F}}_{nn'}^{\lambda\lambda'}(\mathbf{q})$ contains zeros and, therefore, so does Im Π^0 as a function of q at fixed ω. These zeros will play an important role when discussing the structure of the PHES in Sec. III C. Note that $\Pi_n^{\lambda}(\mathbf{q},\omega) = -\Pi_n^{-\lambda}(\mathbf{q},\omega)$ and that the $n=0$ LL does not contribute to the polarization.

III. RESULTS

The dynamical polarization function of graphene, Π_{graph}^0, is now compared to that of the 2DEG, Π_{2DEG}^0.[1] For $B=0$, Π_{graph}^0 has been calculated first in the context of intercalated graphite[6] and later for doped graphene,[8,9] resulting in a particle-hole *continuum* different from that of a 2DEG. The edges of the zero-field PHES for graphene and a 2DEG are drawn as black lines in Fig. 1. While the PHES for a 2DEG is made of a single region limited by linear-parabolic boundaries [see Fig. 1(b)], the PHES in graphene has linear edges and contains two different regions because of intraband (I) and interband (II) processes [see Fig. 1(a)]. The spectral weight in graphene is concentrated around the diagonal $\omega = v_F q$ due to the chirality factor $[1+\lambda\lambda' \cos\theta]/2$,[11] which is the $B=0$ equivalent of Eq. (10).

A. Particle-hole excitation spectrum for noninteracting electrons

In the presence of a magnetic field, the largest contribution to the polarization also comes from the region around $\omega = v_F q$ [see Fig. 1(a)]. In addition, Im $\Pi_{graph}^0(\mathbf{q},\omega)$ is finite not only close to the diagonal but also along regions above and below $\omega = v_F q$ [see the diagonal yellow stripes in Fig. 1(a)]. For comparison, in Fig. 1(b), we show the corresponding density plot[1] of Im $\Pi_{2DEG}^0(\mathbf{q},\omega)$ calculated for the same Fermi momentum $k_F \leftrightarrow \sqrt{2N_F+1}/l_B$.

These results reveal the main differences between the PHES of graphene and that of a 2DEG in the presence of a magnetic field. While the PHES for a 2DEG [Fig. 1(b)] features a set of well-defined *horizontal* lines, with a slight

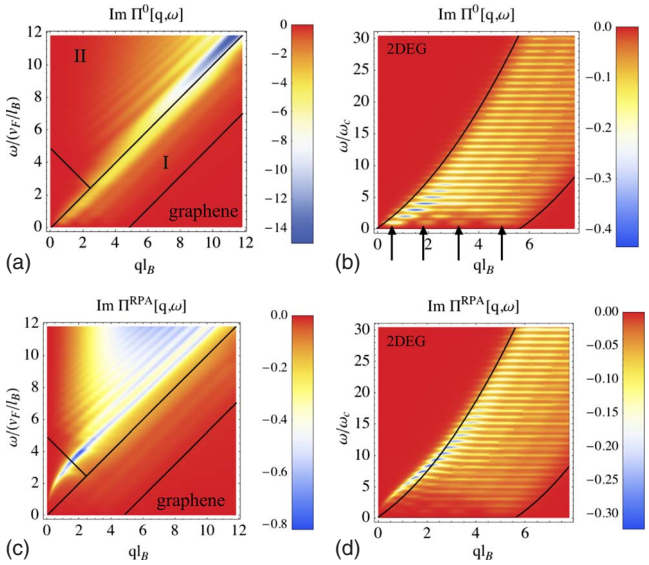

FIG. 1. (Color online) Density plot of the spectral function Im $\Pi(\mathbf{q},\omega)$ for doping $N_F=3$, ultraviolet cutoff $N_c=70$, and disorder broadening $\delta = 0.2 v_F/l_B$ for graphene [panels (a) and (c)] and $\delta = 0.2\omega_c$ for a standard 2DEG [(b) and (d)]: in the absence of interactions [(a) and (b)] and including interactions in the RPA [(c) with $r_s \simeq 1$ and (d) with $r_s \simeq 3$]. The solid lines indicate the zero-field limits of the PHES and arrows point to the *islands* discussed in the text. In panel (a), label I (II) indicates the intraband (interband) region of the PHES in graphene.

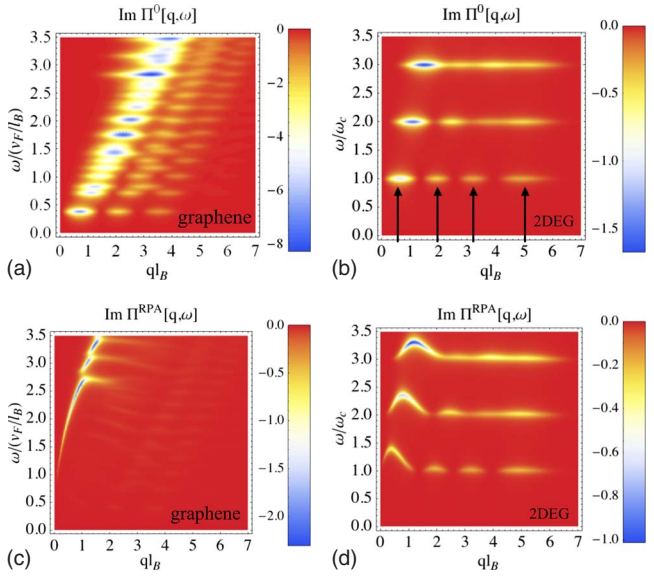

FIG. 2. (Color online) Density plot of Im $\Pi(\mathbf{q},\omega)$ for the low-energy region, for doping $N_F=3$ and ultraviolet cutoff $N_c=70$. Panels (a) and (c) correspond to graphene, whereas (b) and (d) correspond to a 2DEG. The disorder broadening $\delta=0.05$ in units of v_F/l_B and ω_c, respectively, and the interaction strength $r_s \simeq 1$ in panels (c) and (d). Notice the different energy scale with respect to Fig. 1. Arrows indicate islands as discussed in the text.

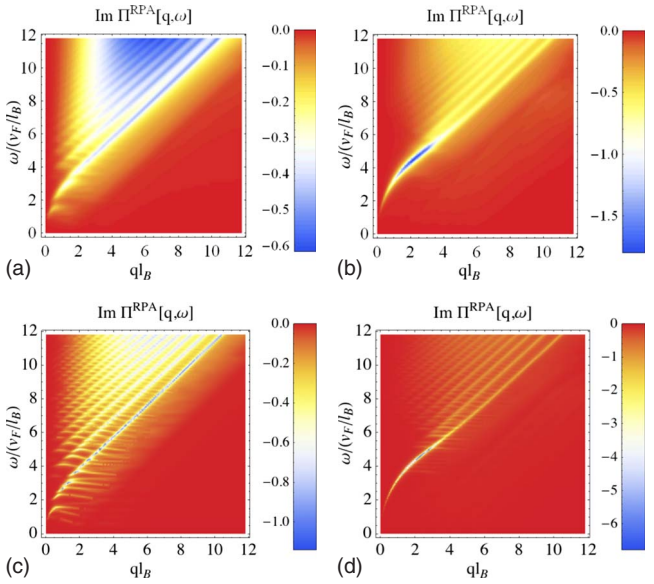

FIG. 3. (Color online) Density plot of Im $\Pi^{\mathrm{RPA}}(\mathbf{q},\omega)$ for graphene, for disorder broadening $\delta=0.2v_F/l_B$ [plots (a) and (b)] and $\delta=0.05v_F/l_B$ [plots (c) and (d)], and doping $N_F=1$ in plots (a) and (c), and $N_F=6$ in plots (b) and (d).

modulation parallel to the boundaries of the particle-hole continuum, that of graphene is remarkably different. Indeed, its PHES [Fig. 1(a)] is *dominated* by this modulation, visible as bright regions in the diagonal, whereas the horizontal lines are now hardly visible, as a consequence of the nonequidistant LL spacing and the presence of a finite disorder broadening δ, as discussed in more detail below (see Sec. III C). The PHES is, thus, discretized into *diagonal* lines (almost parallel to $\omega=v_F q$) in the (q,ω) plane. For Fig. 1, we have chosen $\delta=0.2v_F/l_B$, which is a realistic value for the currently realized graphene samples.[21] Lower values of δ lead to a clearer definition of the horizontal lines [see Fig. 2(a) for a zoom of the low-energy region of the PHES in a cleaner system].

B. Particle-hole excitation spectrum for interacting electrons (RPA)

Electron-electron interactions yield coherent modes that emerge, both in the 2DEG and in graphene, from the regions of highest weight in the PHES. Within the RPA, the renormalized polarization function is given by

$$\Pi^{\mathrm{RPA}}(\mathbf{q},\omega)=\frac{\Pi^0(\mathbf{q},\omega)}{1-v(\mathbf{q})\Pi^0(\mathbf{q},\omega)},$$

where $v(\mathbf{q})=2\pi e^2/\varepsilon_b|\mathbf{q}|$ is the unscreened 2D Coulomb potential, ε_b the dielectric constant, and intervalley processes, which are suppressed in a/l_B, are neglected.[22] The results are shown in Figs. 1(c) and 2(c) for graphene (with $r_s \equiv e^2/\varepsilon_b v_F \approx 1$) and in Figs. 1(d) and 2(d) for a 2DEG (with $r_s \equiv 2m_b e^2/\varepsilon_b k_F \approx 1$ or 3). In the 2DEG, Coulomb interactions lead to the appearance of dispersive magnetoexcitons [see Fig. 2(d)], whereas in graphene, the diagonal lines of the noninteracting PHES [Fig. 1(a)] become coherent collective modes: linear magnetoplasmons that are now clearly visible as peaks in the spectral function. They disperse roughly parallel to $\omega=v_F q$ and are more pronounced in the interband region of the PHES [see Fig. 1(c)]. Notice that even in cleaner samples [$\delta=0.05v_F/l_B$, Fig. 2(c)], the horizontal structure due to the LL quantization is highly suppressed in Im $\Pi^{\mathrm{RPA}}(\mathbf{q},\omega)$. Furthermore, there has been a transfer of spectral weight from the long-wavelength region of the noninteracting PHES to the upper-hybrid mode that starts dispersing in the gapped region of the spectrum [see Fig. 2(c)]. In a 2DEG, this upper-hybrid mode[4] can be seen as the plasmon mode modified by the magnetic field. It is a plasmon-cyclotron collective mode that has a dispersion relation $\omega=[\omega_c^2+\omega_p^2]^{1/2}$, where $\omega_p \approx \sqrt{\epsilon_F e^2 q/\varepsilon_b}$ in the long-wavelength limit. As it is the most intense mode, its square-root behavior is clearly visible in Fig. 1(d) [in Fig. 2(d) it only appears as a maximum in the magnetoexcitons dispersion relation] and also in Figs. 1(c), 2(c), 3(b), and 3(d) for graphene.

C. Discussion

The structure of the PHES in graphene and the 2DEG may be understood in the following manner. First, one notices that the boundaries (black lines in Fig. 1) are due to the momentum conservation of the electron-hole pairs. The boundaries reflect the different $B=0$ behavior of the dispersion relations in graphene (linear in q) as compared to the 2DEG (quadratic in q). Second, for $B\neq 0$, the zero-field continuum becomes chopped into horizontal lines. The main difference between the PHES in the 2DEG and that in graphene stems from the different LL quantization.

In the case of the 2DEG, one notices a constant spacing of the horizontal lines, $\omega=m\omega_c$. There are several contributions

to each horizontal line from the allowed LL transitions, $n \rightarrow n'$, with $m=n'-n$. For a given integer m, the number of contributing LL transitions is the minimal value $\min\{N_F+1,m\}$ of N_F+1 and m. The lowest-energy horizontal line ($m=1$), thus, arises from a single LL transition, $N_F \rightarrow N_F+1$. In this case, the line consists of N_F+1 well-separated *islands* [see arrows in Figs. 1(b) and 2(b)], which is the name we give to regions of high spectral weight, and which are separated by regions of low spectral weight reflecting the nodes of the LL wave functions. For larger values of m, several LL transitions $n \rightarrow n'$ contribute to the same horizontal line. Each of these transitions has $n+1$ islands. Because this number is different for each transition, the islands that arise from different transitions overlap and fill in the region of low spectral weight. As a result, the horizontal lines appear continuous [compare the $m=1$ and $m=3$ horizontal lines in Figs. 1(b) and 2(b)] and the node structure of the LL wavefunction is visible only in form of faint shadows parallel to the boundaries of the PHES [see Figs. 1(b) and 2(d)].

In graphene, the *relativistic* LL quantization gives rise to horizontal lines at energies

$$\omega = v_F l_B^{-1}[\sqrt{2n'} - \lambda\sqrt{2n}], \tag{11}$$

where we have assumed that the Fermi energy lies in the conduction band, an therefore $\lambda'=1$. In contrast to the 2DEG, with equally spaced LLs, only a single transition λ, $n \rightarrow n'$ contributes to each horizontal line. As a consequence, the node structure of the LL wave functions, and therefore that of the form factor (10), is clearly visible in every horizontal line and not only in the one of lowest energy [see Fig. 2(a)]. This explains the presence of $n+1$ islands in the horizontal line corresponding to the $n \rightarrow n'$ transition. These nodes give rise to well-defined diagonal dark lines of low spectral weight parallel to the boundaries of the particle-hole continuum. Another consequence of the relativistic LL structure is that the density of horizontal lines increases with energy, contrary to the case of the 2DEG, where all lines are separated by the constant cyclotron energy [compare Figs. 2(a) and 2(b)]. This clear separation of islands at any energy, together with the rather large number of horizontal lines and their finite disorder-induced width, leads to a stacking of the islands of different energies. This is the origin of the appearance of diagonal regions of strong spectral weight [see Figs. 1(a) and 2(a)]. The overlap of islands of different energies is stronger for higher values of disorder in the sample (increased LL broadening δ) as well as for higher filling factors. The relative energy separation between the horizontal lines will be smaller for larger N_F, because in the single-particle graphene spectrum, the density of LLs increases with energy. Electron-electron interactions turn these original regions of strong spectral weight into coherent excitations (the upper-hybrid mode and the linear magnetoplasmons). In fact, we have studied the PHES of graphene for different values of doping (i.e., $N_F \neq 3$) and disorder broadening δ and found that the physical picture exposed above is unaltered (see Fig. 3). As a general rule, disorder and doping favor the emergence of linear magnetoplasmons in graphene as compared to the horizontal magnetoexcitons. For the experimentally relevant values of δ and N_F, linear magnetoplasmons therefore dominate the PHES of graphene in the integer quantum-Hall regime. It is worth noticing that, at fixed carrier density, increasing the filling factor ($\sim N_F$) is equivalent to effectively lowering the magnetic field. Although Fig. 3 represents the PHES at fixed values of v_F/l_B, i.e., fixed magnetic field, one easily sees that at larger values of N_F, most of the spectral weight is concentrated in the upper-hybrid mode [see Fig. 3(d)]. This mode is the only collective excitation in the integer quantum-Hall regime that evolves continuously into the plasmon mode at zero field. In contrast to the upper-hybrid mode, the linear magnetoplasmons become less intense in the large N_F limit and evolve for $B \rightarrow 0$ into the incoherent particle-hole continuum.

IV. CONCLUSIONS

In conclusion, the magnetic field particle-hole excitation spectrum in graphene has been investigated and the results have been compared to those of a standard 2DEG with a parabolic band dispersion. Most saliently, the particular LL quantization in graphene yields linear magnetoplasmon modes, which are not captured in the usual magnetoexciton approximation. This is due to the fact that a single-particle hole process contributes to a given energy in graphene, whereas for a 2DEG, there are, in general, many processes contributing to the same energy. As a consequence, the node structure of the LL wave functions in graphene is evident at any energy of the PHES, leading to a particular spectrum where the relevant modes are diagonal, dispersing roughly parallel to $v_F q$. The dominant role of linear magnetoplasmons is enhanced by doping and Landau-level broadening due to disorder. In addition to linear magnetoplasmons, electron-electron interactions give rise to the upper-hybrid mode as well, which is the plasmon mode renormalized by the magnetic field. This alternative scenario of linear magnetoplasmons, as opposed to horizontal magnetoexcitons, may find an experimental proof in the framework of microwave absorption or inelastic (Raman) light scattering, which has proven to be a powerful tool for measuring the collective excitations of the 2DEG in a strong magnetic field, see, e.g., Ref. 23.

ACKNOWLEDGMENTS

We thank Y. Gallais, P. Lederer, and F. Piéchon for useful discussions and acknowledge funding from the ANR under Grant No. ANR-06-NANO-019-03 and "Triangle de la Physique."

[1] G. F. Giuliani and G. Vignale, *Quantum Theory of the Electron Liquid* (CUP, Cambridge, 2005).
[2] D. Pines and P. Nozières, *The Theory of Quantum Liquids* (W. A. Benjamin, Inc., New York, 1966).
[3] C. Kallin and B. I. Halperin, Phys. Rev. B **30**, 5655 (1984).
[4] K. W. Chiu and J. J. Quinn, Phys. Rev. B **9**, 4724 (1974); T. H. Styx, *Theory of Plasma Waves* (McGraw-Hill, New York, 1962).
[5] A. H. C. Neto, F. Guinea, N. M. R. Peres, K. Novoselov, and A. K. Geim, Rev. Mod. Phys. **81**, 109 (2009).
[6] Kenneth W.-K. Shung, Phys. Rev. B **34**, 979 (1986).
[7] J. González, F. Guinea, and M. A. H. Vozmediano, Nucl. Phys. B **424**, 595 (1994).
[8] B. Wunsch, T. Stauber, F. Sols, and F. Guinea, New J. Phys. **8**, 318 (2006).
[9] E. H. Hwang and S. Das Sarma, Phys. Rev. B **75**, 205418 (2007).
[10] J. Sabio, J. Nilsson, and A. H. Castro Neto, Phys. Rev. B **78**, 075410 (2008).
[11] M. Polini, R. Asgari, G. Borghi, Y. Barlas, T. Pereg-Barnea, and A. H. MacDonald, Phys. Rev. B **77**, 081411(R) (2008).
[12] E. H. Hwang and S. Das Sarma, Phys. Rev. B **77**, 081412(R) (2008).
[13] K. S. Novoselov, A. K. Geim, S. V. Morozov, D. Jiang, M. I. Katsnelson, I. V. Grigorieva, S. V. Dubonos, and A. A. Firsov, Nature (London) **438**, 197 (2005).
[14] Y. Zhang, Y.-W. Tan, H. L. Stormer, and P. Kim, Nature (London) **438**, 201 (2005).
[15] A. Iyengar, J. Wang, H. A. Fertig, and L. Brey, Phys. Rev. B **75**, 125430 (2007).
[16] Y. A. Bychkov and G. Martinez, Phys. Rev. B **77**, 125417 (2008).
[17] K. Shizuya, Phys. Rev. B **75**, 245417 (2007).
[18] M. Tahir and K. Sabeeh, J. Phys.: Condens. Matter **20**, 425202 (2008).
[19] O. L. Berman, G. Gumbs, and Y. E. Lozovik, Phys. Rev. B **78**, 085401 (2008).
[20] The continuum approximation is valid up to an energy $\sim t$. This leads to a cutoff in the Landau-level index $N_c \sim 10^4/B[T]$. As the LL separation in graphene decreases with n, it is possible to have *semiquantitative* results from smaller values of N_c. Here, for numerical calculations, we typically take $N_c \approx 70$. There are no noticeable differences for larger values of N_c.
[21] T. Ando, J. Phys. Soc. Jpn. **76**, 024712 (2007).
[22] M. O. Goerbig, R. Moessner, and B. Douçot, Phys. Rev. B **74**, 161407(R) (2006).
[23] M. A. Eriksson, A. Pinczuk, B. S. Dennis, S. H. Simon, L. N. Pfeiffer, and K. W. West, Phys. Rev. Lett. **82**, 2163 (1999).